Progress in Oceanography 248 (2026) 103810

Contents lists available at ScienceDirect

Progress in Oceanography

journal homepage: www.elsevier.com/locate/pocean

Variations in phytoplankton photosynthetic parameters around the subsurface chlorophyll maxima in the eastern Indian Ocean revealed by high-resolution measurements

Mitsuhide Sato [a,b,*], Takako Masuda [c], Yoshiko Kondo [a], Takuya Sato [d,e], Hiroaki Saito [b]

[a] Graduate School of Integrated Science and Technology, Nagasaki University, Bunkyo-machi 1-14, Nagasaki-shi, Nagasaki, Japan
[b] Atmosphere and Ocean Research Institute, The University of Tokyo, Kashiwanoha 5-1-5, Kashiwa-shi, Chiba, Japan
[c] Fisheries Research Institute, The Japan Fisheries Research and Education Agency, Shinhama-cho 3-27-5, Shiogama-shi, Miyagi, Japan
[d] Institute for Chemical Research, Kyoto University, Gokasho, Uji-shi, Kyoto, Japan
[e] Graduate School of Agricultural and Life Sciences, The University of Tokyo, Yayoi 1-1-1, Bunkyo-ku, Tokyo, Japan

ARTICLE INFO

Keywords:
Eastern Indian Ocean
Single turnover active fluorometry
Subsurface chlorophyll maximum
Light-iron co-limitation

ABSTRACT

Despite substantial variations in the physicochemical and biological environments around the subsurface chlorophyll maximum (SCM), how photosynthetic parameters vary around the SCM has been scarcely studied. To reveal the fine-scale profiles of photosynthetic parameters and their controlling mechanisms, seawater samples collected at approximately 3-m vertical intervals in the eastern Indian Ocean were analyzed using single turnover active fluorometry (STAF), together with other environmental parameters. The saturation irradiance of photosynthesis was higher than the *in situ* average irradiance of photosynthetically active radiation during the daytime throughout the sampled layers, indicating that the subsurface phytoplankton communities were under suboptimal light conditions. Throughout the studied depths, the initial slope of the photosystem II photochemical flux – irradiance curve (α-value) and maximum quantum yield of photosystem II (F_v/F_m) increased with depth, while non-photochemical quenching (NPQ_{NSV}) decreased, suggesting relief from photoinhibition and nutrient stress with depth. In addition to these general trends, at the three stations between the equator and 21°S, local minima of α and F_v/F_m values were observed around the SCM, along with increased NPQ_{NSV}, suggesting the enhanced physiological stress on photosynthesis by phytoplankton communities around the SCM in the eastern region of the South Indian Subtropical Gyre. These local variations were significantly correlated with the chlorophyll concentration and could not be explained by changes in solar irradiance or macronutrient availability. In addition to changes in phytoplankton community composition, one possible cause is iron deficiency under light limitation, which is sometimes observed in stratified subtropical waters. However, further examination in this area is required. These local variations in photosynthetic parameters can result in lower carbon fixation rates around the SCM in the eastern Indian Ocean compared to estimates based on relief from light and macronutrient limitations.

1. Introduction

Ocean primary production, which is primarily fueled by phytoplankton, plays an important role in global carbon fixation and climate regulation. Model calculations based on satellite ocean color imaging have contributed to the estimation of global-scale phytoplankton biomass and productivity at various spatiotemporal scales (Behrenfeld et al., 2006a). Chlorophyll concentration, which is used as an index of phytoplankton biomass and as a unit of primary production, often shows a subsurface chlorophyll maximum (SCM), particularly in stratified open oceans (Anderson, 1969; Saijo et al., 1969). Various explanations have been proposed for the formation and maintenance of SCM (Cornec et al., 2021), including active growth (Masuda et al., 2010), photoacclimation (Letelier et al., 2004; Masuda et al., 2021), passive accumulation (Varela et al., 1992; Murty et al., 2000), and light-dependent grazing (Moeller et al., 2019).

In addition to chlorophyll concentration, primary productivity shows a subsurface maximum in various waters, including the North Sea

* Corresponding author at: Graduate School of Integrated Science and Technology, Nagasaki University, Bunkyo-machi 1-14, Nagasaki-shi, Nagasaki, Japan.
E-mail address: satom@g.ecc.u-tokyo.ac.jp (M. Sato).

https://doi.org/10.1016/j.pocean.2026.103810
Received 10 December 2025; Received in revised form 30 June 2026; Accepted 14 August 2026
Available online 14 August 2026

(Weston et al., 2005), Arctic Sea (Palmer et al., 2013), Mediterranean Sea (Marañón et al., 2021), Bay of Bengal (Liu et al., 2011), and Antarctic Polar Front (Tripathy et al., 2015; Kerkar et al., 2020), although the peak depths are often shallower than those of the SCM. In contrast, in chronically stratified subtropical gyres, the subsurface peak in primary production is less pronounced and often absent (DiTullio et al., 2003; Chen, 2005; Pérez et al., 2006).

These differences in the vertical profiles of primary production likely reflect the differences in the photophysiological status of subsurface phytoplankton communities, which can be determined using photosynthetic parameters (Zhu et al., 2017). Vertical profiles of photosynthetic parameters in the Indian Ocean demonstrate a reduced quantum yield of photosystem II (PSII) at the surface, likely due to nitrogen limitation, whereas light limitation has been suggested for subsurface waters (Wei et al., 2019; Yuan et al., 2019). Similar patterns have been observed at the Antarctic Polar Front, where severe iron limitation is likely to occur at the surface (Kerkar et al., 2020). In these areas, the strength of light limitation around the SCM is considered a determinant of potential primary productivity. Therefore, measuring photosynthetic parameters is effective for estimating phytoplankton primary productivity in subsurface waters and its controlling factors.

Around the SCM, vertical variations in environmental conditions influence the physiological status of phytoplankton, which in turn alter chlorophyll concentrations and phytoplankton community structure with depth (van den Engh et al., 2017; Sato et al., 2022a). Although SCM has been the focus of ocean observations, sampling intervals around it are typically 10 m or wider, which may result in a failure to grasp possible vertical variations in environmental parameters (e.g., nutrient concentrations) around the SCM. Additionally, the SCM often moves vertically along an isotherm or isopycnal (Ryabov et al., 2010; Zampollo et al., 2023), which may result in a failure to collect samples from the exact SCM depth when the sampling density is insufficient. These problems can be addressed through semi-continuous observations using a mooring fluorometer, which enables high-resolution data collection from the water column (Bibby et al., 2008; Cheah et al., 2013; Kerker et al., 2020; Wang et al., 2024). High-frequency sampling is also effective for collecting data from the SCM (van den Engh et al., 2017; Sato et al., 2022b).

In this study, we conducted high-frequency sampling around the SCM, along a latitudinal transect in the eastern Indian Ocean during the late boreal summer monsoon season. In the subtropical and tropical regions of this area, the SCM developed between 50 and 100 m, the magnitude and depth of which vary seasonally (Argo, 2000; Fig. S1), whereas in the transition area south of 30 °S, the SCM appeared only during the austral summer, from December to April. We measured phytoplankton photosynthetic parameters using a benchtop fluorometer, along with relevant environmental parameters, to reveal their high-resolution vertical structure. The results elucidate the fine-scale vertical

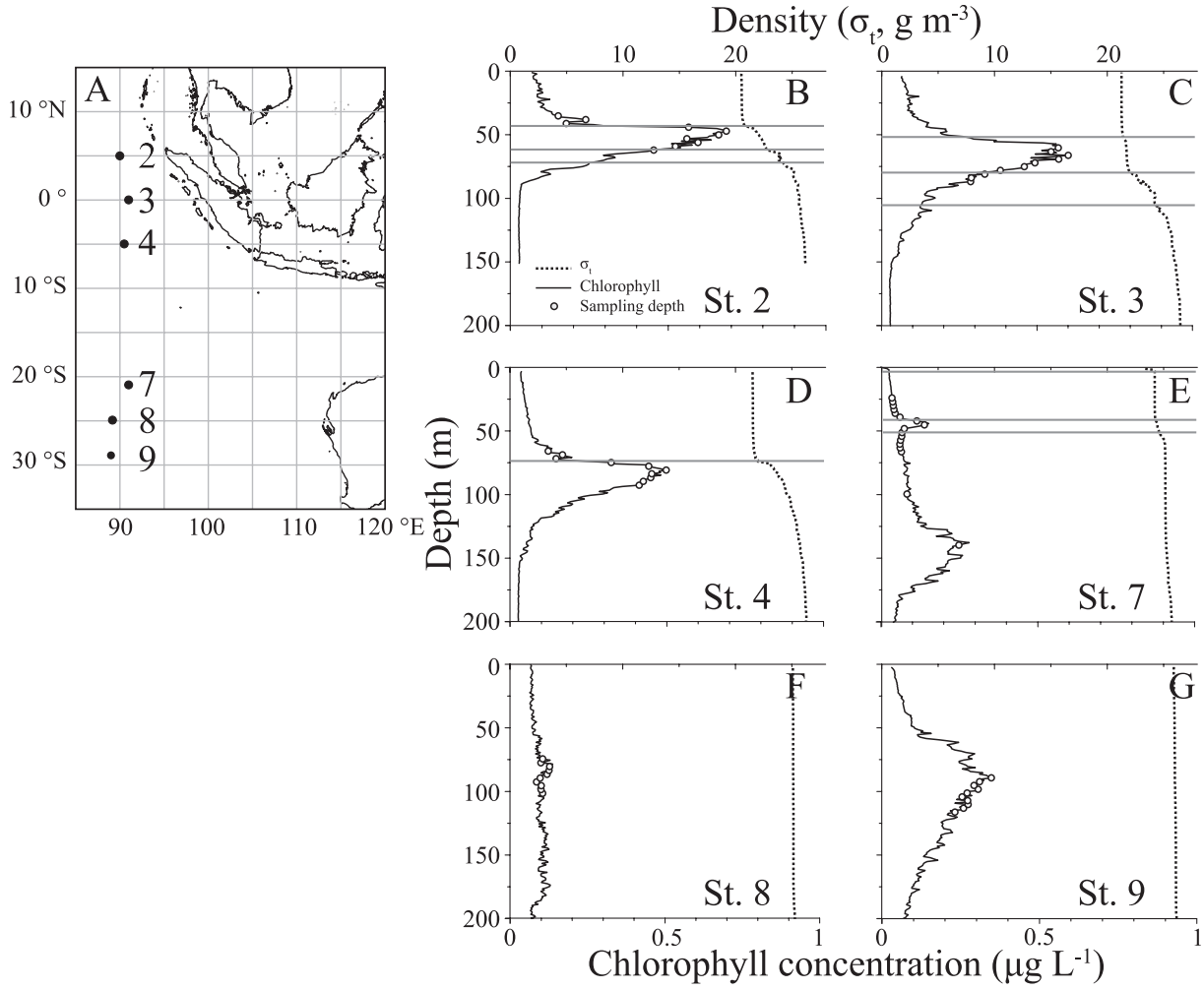

Fig. 1. Station map (A) with vertical profiles of relative density (σ_t, g m^{-3}, dotted line) and chlorophyll concentration (μg L^{-1}) in the upper 200 m of the water column at each sampling station (B – G). Chlorophyll fluorescence was converted into chlorophyll *a* concentration by linear regression against the fluorometrically determined concentrations in extracted samples (see Materials and Methods). Depths at which seawater samples were collected by high-resolution sampling are shown as blank circles. Pycnoclines are shown by horizontal gray lines.

variations in phytoplankton physiological status around the SCM, obtained via high-resolution sampling and fluorometric determination of photosynthetic parameters.

2. Materials and methods

2.1. Sampling

Samples were collected from a latitudinal transect at 90 °E during the KH-24-3 research cruise of the R/V Hakuho-maru from August to September 2024 in the late summer monsoon season (Fig. 1). High-resolution sampling was conducted using Niskin-X samplers attached to a carousel multisampling system. Vertical profiles of temperature, salinity, chlorophyll fluorescence, and dissolved oxygen concentrations were obtained using a conductivity-temperature-depth (CTD) sensor. The depth of the SCM was obtained from the vertical profile of chlorophyll fluorescence during the downward cast, and the sampling depth range was determined. During the upward cast, the sampling carousel was fired at approximately 3-m intervals within the predetermined sampling range, with the cable slowly winched up at a rate of < 0.3 m s^{-1} (typically 0.1 m s^{-1}). The winding rate was chosen as a tradeoff to minimize effects of ship motion due to surface and internal waves, and to minimize water entrainment during the rosette motion. Sampling times varied at different stations (Table 1).

After retrieving the water samples, subsamples were collected for flow cytometry, nutrients (including nitrate, nitrite, ammonium, soluble reactive phosphorus, and silicic acid), and photosynthetic parameter analyses. Samples for flow cytometry and photosynthetic parameters were collected in acid-cleaned 125-mL black polyethylene bottles. For flow cytometry, 4-mL aliquots were dispensed into cryovial tubes, fixed with 1% glutaraldehyde, and frozen at −80 °C (Vaulot et al., 1989; Sato et al., 2006) in a freezer. As liquid nitrogen was not used for freezing, some phytoplankton taxa may have been lost during freezing. The remaining aliquots were dispensed into 30-mL polyethylene tubes and kept in a dark water tank controlled at the temperature at the SCM depth obtained from a CTD data profile, until fluorometric analysis of the photosynthetic parameters was performed on board. Nutrient samples were collected in duplicate in 10-mL acrylic tubes without filtration. The samples were stored frozen at −20 °C in a polyethylene ziplock bag until further laboratory analysis.

As a trace-metal-clean technique was not employed in this study, samples of trace metals, including iron, were not collected. To avoid changes in the physiological status of the phytoplankton due to potential trace metal contamination, the samples were processed or analyzed as soon as possible after collection.

2.2. Measurement of photosynthetic parameters

Photosynthetic parameters were measured at each depth using single-turnover active fluorometry with a benchtop fluorometer (LabSTAF, Chelsea Technologies, UK). Samples were dark-acclimated prior to measurement to ensure complete relaxation of non-photochemical quenching (NPQ) and stabilization of the fluorescence signals. Fluorometry was initiated within approximately 1 h of collection, except at St. 2, and was completed within 5 h (Table 1) to minimize the effects of possible trace metal contamination on the photosynthetic physiology of phytoplankton and standardize the photosynthetic state across samples collected at different times and depths. This extended dark-acclimation period allowed the assessment of the maximum photochemical efficiency of PSII under fully relaxed conditions. Although such a treatment may reduce short-term variability associated with *in situ* light history, it provides a consistent baseline for comparing the intrinsic photosynthetic capacity of phytoplankton assemblages across depths.

A single-turnover (ST) saturation phase was applied with a solid flash of 100 μs to measure the minimal and maximal fluorescence yields, as described by Boatman et al. (2019). Samples were subsequently exposed to eight sequential levels of photosynthetically active radiation (PAR) using the auto FLC mode at 120-s intervals to obtain a fluorescent light curve. The electron transport rate - irradiance (ETR-E) relationships were derived from the fluorescence light curves at eight irradiance levels using the auto-FLC mode of the LabSTAF instrument. The LabSTAF fluorometer was operated using a 452-nm blue LED for all measurements. The same excitation and measurement protocols were applied to all samples at all depths and stations. The maximum actinic photon irradiance varied from 243 to 1826 μmol photons^{-1} m^{-2} s^{-1}.

Measurements obtained during the dark step (Step 1) provided the minimal (F_0) and maximal (F_m) fluorescence intensities. After correcting for the background fluorescence of filtered seawater prepared using a DISMIC syringe filter (Advantec, cellulose acetate, 0.2-μm pore size), the maximum quantum yield of PSII ($F_v/F_m = (F_m - F_0) / F_m$) was determined for each sample. The fluorescence signals from the filtered seawater were typically <10% of those from the unfiltered samples, with negligible variation between different depths.

Minimal (F') and maximal (F_m') fluorescence were recorded, and the effective fluorescence yield of PSII ($F_q'/F_m' = (F_m' - F') / F_m'$) was calculated (Kolber et al., 1998; Oxborough et al., 2000) for each light step. Simultaneously, the effective absorption cross-section of PSII (σ'_{PSII}) was obtained. The parameters obtained under each light step were used to calculate the PSII photochemical fluxes per unit volume per unit time (JV_{PII}) (Schuback et al., 2024). Non-photochemical quenching (NPQ_{NSV}) was calculated as described by Schuback et al. (2015). The packaging effect correction was implemented internally by RunSTAF using the correction factor (cPEC), which was derived from dual-waveband fluorescence measurements. According to LabSTAF workflow, cPEC was applied to the absorption coefficient for PSII light harvesting (a_{LHII}) and the corrected a_{LHII} values were subsequently used for the calculation of JV_{PII} (Oxborough, 2022). In the present study, the cPEC values ranged from 0.7169 to 8.116 (mean = 1.847 ± 1.830, n =

Table 1
The local times of sample retrieval, and the start and end of the LabSTAF measurements. All times were calculated from Greenwich Standard Time and the longitude of the sampling station.

	SCM depth (m)	Sampling range (m)	Sample retrieval (local time)	Measurement start (local time)	Measurement end (local time)	Surface temperature (°C)	Mixed layer depth (m)
St. 2	47	35-62	17:52	5:37	8:59	29.5	22
St. 3	64	58-85	15:28	16:39	19:48	29.5	51
St. 4	80	65-92	11:12	11:30	14:18	28.5	64
St. 7	45	25-67	10:56	11:25	15:44	22.6	39
St. 8	N/A	75-102	18:10	18:58	21:44	20.8	99
St. 9	104	89-116	9:15	10:17	12:52	18.2	23

66). The observed variability in cPEC values likely reflects the natural variations in cell size, pigment packing, and community composition. Higher values may occur in assemblages with larger cells or higher pigment concentrations, which enhance fluorescence reabsorption effects.

The initial slope (α-value) and saturation irradiance (E_k) were obtained from relationship between JV_{PII} and actinic photon irradiance at eight different light levels. The fitting procedure was implemented within the software based on the general framework of photosynthesis-irradiance (P-E) relationships (Platt and Gallegos, 1980), although the specific functional form was not explicitly defined by the manufacturer. This approach is consistent with the standard implementation of STAF-based light response analyses. E_k represents the irradiance at which photosynthesis transitions from light-limited to light-saturated conditions. All curves are provided in the Supplementary Materials (Fig. S2).

2.3. Measurement of other parameters

Flow cytometry was performed on samples thawed at room temperature using a benchtop flow cytometer (CytoFLEX; Beckman Coulter) equipped with dual lasers (405 nm [violet] / 488 nm [blue]). In addition to the forward and side light scatter from the blue laser, the side scatter from the violet laser was collected to improve the resolution of small particles, including the pico-sized cyanobacteria *Prochlorococcus* (Brittain et al., 2019). Orange (590–630 nm) and red (640–740 nm) fluorescence intensities excited by a blue laser were employed in combination with light scattering to distinguish between three pico- and nanophytoplankton populations: *Synechococcus*, *Prochlorococcus*, and eukaryotes. Cryptophytes and nano-sized cyanobacteria exhibiting strong orange fluorescence (Sato et al., 2010) were not detected throughout the study area. All the signals were recorded over 10^7 ranges and saved as FCS files. Event counts were converted to volumetric cell concentrations (cells mL^{-1}) based on a pre-calibrated flow rate (approximately 50 μL min^{-1}).

Nutrient concentrations were measured using a conventional colorimetric method with an autoanalyzer (QuAAtro 39, BLTec, Japan). Frozen samples were thawed at room temperature prior to analysis. The concentrations of all five nutrients (nitrate, nitrite, ammonium, soluble reactive phosphorus (SRP), and silicic acid) were calibrated against KANSO-CRM RMNS, a certified reference material produced by KANSO Technos Co., Ltd. This study presents results only for nitrate, nitrite, and SRP.

For comparison with *the* E_k values, the vertical profiles of PAR intensity were estimated from satellite-derived surface PAR irradiance and light extinction measured with a photometer. We calculated the PAR intensity at each depth by multiplying the 8-day-averaged surface PAR intensity by the relative light intensity to the surface intensity. The 8-day-averaged surface PAR data were downloaded from the MODIS-Aqua website (https://oceancolor.gsfc.nasa.gov/) and processed in Python 3.6 using the netCDF4 library. The vertical profile of light extinction within the water column was obtained near midday using a free-falling underwater photometer, PRR800 (Biospherical Inc.), and PAR intensity was measured using a spectral radiometer, PRR810 (Biospherical Inc.), set on the deck as a surface reference. Both photometers were installed with a 2π planar sensor. The daily PAR was converted to the average per-second PAR (μmol photons m^{-2} s^{-1}) by dividing it by the daytime length.

Fine-scale profiles of chlorophyll fluorescence (1-m intervals) were converted into those of extracted chlorophyll *a* concentration (μg L^{-1}) using linear regression of fluorescence values against chlorophyll *a* concentrations from all discrete samples collected during the cruise (Fig. S3, $n = 65$, $R^2 = 0.85$). Because this was a linear conversion, it did not affect the qualitative outcomes of this study.

Statistical tests were performed using OriginPro 2015 (OriginLab) and BellCurve for Excel ver. 4.05 (BellCurve). The level of significance was set at 5% (0.05), unless otherwise specified.

3. Results

A distinct SCM was observed between 50 and 100 m at the three sampling stations in the northern hemisphere and the equator, which almost coincided with a seasonal pycnocline (Fig. 1B, C, and D). At Sts. 2 and 3, the pycnocline comprised three or four steps spanning from 50 to 100 m, and the SCM appeared just below the top of the shallowest pycnocline. In contrast, in the southern hemisphere, a seasonal pycnocline was absent (Fig. 1E, F, and G), likely due to strong mixing during the austral winter, except at St. 7, where two chlorophyll peaks were found in the upper 200 m, and a shallower peak appeared at a depth of approximately 50 m, accompanied by a slight pycnocline (Fig. 1E). The results of the second (deeper) peak at St. 7 were excluded from subsequent analyses. At Sts. 7 and 9, a relatively wide peak in chlorophyll fluorescence was observed, which was not accompanied by a pycnocline (Fig. 1E and F). Considering the extremely low irradiance at these depths, these peaks were likely composed of senescent assemblages that sank into the deep sea and were not sampled in this study.

The 8-day-averaged daily surface PAR irradiance, derived from satellite data at the time of the study, was approximately 40 mol m^{-2} d^{-1}, with no significant variation among the stations in the study area. The estimated average daytime PAR irradiance at the SCM peak was 58, 34, and 23 μmol photons m^{-2} s^{-1} at Sts. 2, 3, and 4, respectively, in the northern hemisphere (Fig. 2). At St. 7, the daytime PAR at the SCM was 119 μmol photons m^{-2} s^{-1}, which was much higher than that in the northern hemisphere. In contrast, at the deep chlorophyll peak observed at St. 9, the daytime PAR was as low as 12 μmol photons m^{-2} s^{-1}. The instant PAR irradiance measured using the underwater photometer was similar to or lower than the estimated 8-day-averaged daily surface PAR irradiance, except at St. 3. These latitudinal differences in daytime PAR irradiance in the SCM may be related to variations in the light extinction coefficient of the water column (Table 3), which reflects the latitudinal gradient of the surface biomass. The extinction coefficient around the SCM was significantly higher at the three northern stations than at the other three stations (Student's *t*-test, $P < 0.005$).

Saturation irradiance (E_k), derived from measurements after dark adaptation, showed a pronounced decrease with depth around the SCM, except at the two southernmost stations, 8 and 9 (Fig. 2, Table 2), indicating a vertically homogeneous photophysiological status of phytoplankton at these two stations owing to strong mixing. In contrast, at St. 7, where water column stratification was still in the early stages (Fig. 1), the logarithm of E_k showed a significant negative correlation with depth, although the slope was smaller than that at the northern stations (Table 3).

The vertical profiles of the initial slope of the P-E curve (α value) and the maximum quantum yield of PSII (F_v/F_m), both of which were estimated from the fluorometric measurements, were well correlated across all six surveyed stations (Fig. 3). At the four northernmost stations, where a distinct SCM was observed, both photosynthetic parameters exhibited a decrease near the SCM peak, which was especially pronounced at Sts. 4 and 7. At St. 8, a slight decline in both parameters was observed at 84 m; however, no apparent association with other environmental parameters was observed. At St. 9, the two parameters showed dynamic variation, which was likely attributable to the low phytoplankton biomass at this station. The F_v/F_m values were consistently lower than the theoretical maximum of 0.65 across all depths and sampling stations. The NPQ_{NSV} vertical profile was largely a mirror image of that of α and F_v/F_m, showing a local maximum around the SCM at the four northern stations, although its vertical trend was less clear than that of α and F_v/F_m, owing to its relatively large deviation.

Two photosynthetic parameters, α and F_v/F_m, were largely negatively correlated with the ambient PAR irradiance (Fig. 4). When analyzed by station, α was significantly negatively correlated with the logarithm of PAR irradiance at Sts. 2, 3, and 7, while the correlation between F_v/F_m and PAR irradiance was significant at Sts. 2 and 3. Analysis of covariance revealed that the slopes of the regression lines were not significantly

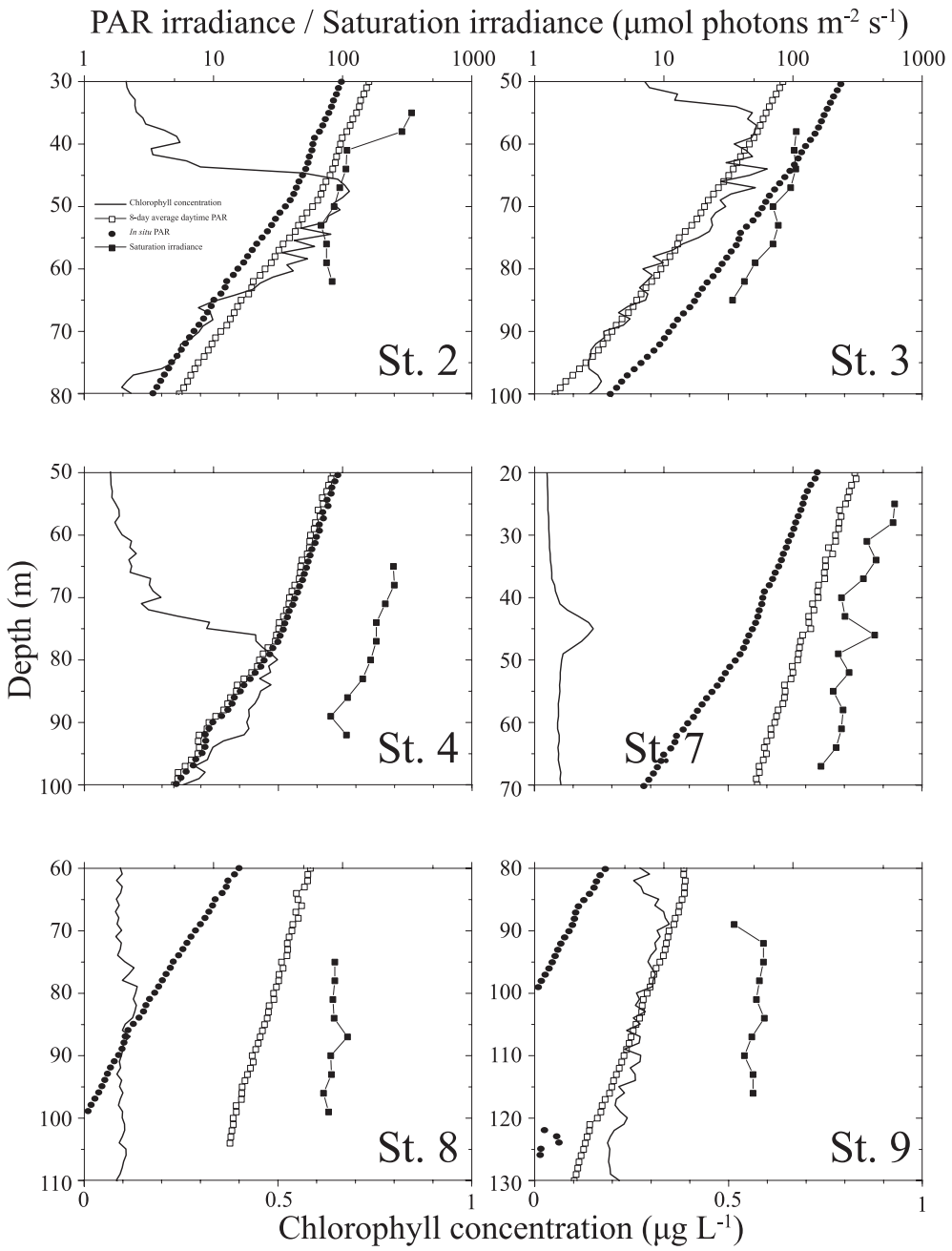

Fig. 2. Vertical profiles of the estimated 8-day-averaged PAR irradiance during daytime (blank squares, μmol photons m^{-2} s^{-1}), *in situ* PAR irradiance measured by an underwater photometer around midday (solid circles, μmol photons m^{-2} s^{-1}), and potential saturation irradiance of photosynthesis (solid squares, μmol photons m^{-2} s^{-1}), estimated by single-turnover active fluorometry (STAF), around subsurface chlorophyll maxima (SCM), along with those of chlorophyll concentration (solid line, μg L^{-1}).

different between stations ($P = 0.15$ for α and 0.38 for F_v/F_m), suggesting that the photosynthetic parameters at these stations were determined by the same mechanism, which was likely driven by light intensity. Interestingly, at St. 7, a sharp negative deviation from the regression line was observed, with a depth corresponding to that of the SCM. At St. 4, the upper three data points were scattered around those at St. 2, 3, and 7, whereas the other data points, which were collected from the wide chlorophyll peak (Fig. 1D), deviated negatively from the regression line.

At Sts. 3, 4, and 7, two photosynthetic parameters, α and F_v/F_m, showed significant negative correlations ($P < 0.05$) with chlorophyll concentration (Fig. 5), suggesting deterioration of the photosynthetic apparatus with the accumulation of phytoplankton pigments at these stations. Although similar negative trends were observed at neighboring Sts. 2 and 8, these were not statistically significant ($P > 0.05$). The slopes of the two parameters at St. 7 were steeper than those at Sts. 3 and 4 (Fig. 5, Table 4). The difference in the slope was significant only at the α value between Sts. 4 and 7 ($P < 0.01$), whereas the slope of F_v/F_m against chlorophyll concentration at St. 7 was significantly higher than that at Sts. 3 and 4 ($P < 0.001$). The steeper slope at St. 7 suggested greater physiological stress on the phytoplankton communities there.

The phytoplankton community around the SCM was numerically dominated by *Prochlorococcus* at all stations surveyed in this study, whereas the relative dominance of each of the three phytoplankton populations varied both vertically and horizontally (Fig. 6). Interestingly, the abundance peak of each phytoplankton population was not distinctly observed; even when observed, it was sometimes displaced

Table 2
Summary of photosynthetic parameters obtained by LabSTAF measurements. All parameters are depicted as averages (ranges).

	Saturation irradiance (E_k, μmol photons m^{-2} s^{-1})	Initial slope of P-E curve (α, m^{-1})	Maximum quantum yield of PSII (F_v/F_m)	Non-photochemical quenching (NPQ_{NSV})
St. 2	133 (68–342)	0.265 (0.237–0.329)	0.38 (0.32–0.43)	1.20 (0.75–1.68)
St. 3	75 (34–106)	0.335 (0.283–0.413)	0.40 (0.36–0.44)	1.31 (0.62–1.73)
St. 4	168 (81–251)	0.251 (0.217–0.320)	0.35 (0.31–0.41)	1.89 (0.71–2.58)
St. 7	324 (165–613)	0.270 (0.181–0.317)	0.35 (0.26–0.41)	1.70 (0.49–3.56)
St. 8	85 (71–109)	0.248 (0.212–0.284)	0.35 (0.30–0.40)	1.58 (0.92–1.85)
St. 9	51 (35–60)	0.208 (0.179–0.273)	0.31 (0.26–0.41)	1.83 (0.09–2.41)

Table 3
Attenuation coefficients (logarithmic slopes) of photosynthetic saturation irradiance and photosynthetically active irradiance against depth at each station. The values are shown only when the regression was statistically significant ($P < 0.05$). All the values are shown with 95% confidence intervals.

	Slope of E_k (m^{-1})			Slope of PAR (m^{-1})		
St. 2	−0.051	±	0.013	−0.066	±	0.002
St. 3	−0.042	±	0.005	−0.080	±	0.000
St. 4	−0.040	±	0.005	−0.068	±	0.002
St. 7	−0.025	±	0.004	−0.036	±	0.000
St. 8	Insignificant ($P > 0.05$)			−0.036	±	0.001
St. 9	Insignificant ($P > 0.05$)			−0.042	±	0.000

from the SCM. For example, at Sts. 2 and 4, the subsurface peaks of eukaryotes largely coincided with the SCM, whereas the peaks of the other two populations, *Synechococcus* and *Prochlorococcus*, appeared at shallower depths. At St. 3, all three populations exhibited similar vertical profiles. The cell concentrations were higher around the SCM than at other depths. However, it was unclear whether their peaks coincided with the SCM because of the sampling depth range at this station. At St. 7, the vertical variation in cell concentrations around the SCM was minimal, except for eukaryotes, which showed an acute abundance peak in the SCM. In addition to these vertical variations in cell concentration, changes in cellular chlorophyll content, as inferred from the cellular red (chlorophyll) fluorescence (Fig. S4), could account for the formation of the SCM at these stations. Cellular chlorophyll fluorescence of *Synechococcus* and *Prochlorococcus* increased with depth around the SCM at Sts. 2, 4, and 7, suggesting their photoacclimation and photoadaptation in a stratified water column. In contrast, the cellular chlorophyll fluorescence of eukaryotes decreased with depth, which was likely attributable to a concurrent decrease in their average cell size, as inferred from decreases in the forward scatter (Fig. S5).

At Sts. 8 and 9, where the water column was well mixed, the abundance of *Synechococcus* was vertically constant, which was typical for the well-mixed water column. However, the vertical profiles at St. 9 revealed that *Prochlorococcus* and eukaryotes showed a small peak in abundance between 90 and 100 m, which corresponded to a slight peak in chlorophyll fluorescence. In contrast, there were no discernible peaks in the abundance of each phytoplankton population at St. 8. However, the cellular chlorophyll fluorescence of *Prochlorococcus* and *Synechococcus* was higher between 80 and 90 m, which may account for a slight increase in total chlorophyll fluorescence. These fine-scale profiles of phytoplankton abundance and optical properties demonstrate that even in a well-mixed water column, where physical conditions appear vertically homogeneous, meter-scale heterogeneity in phytoplankton communities can occur, likely owing to the heterogeneous distribution of resources, including nutrients, organic matter, and light.

The vertical patterns of nutrient concentrations were markedly different between the northern (Sts. 2, 3, and 4) and southern (Sts. 7, 8, and 9) stations (Fig. 7). At the three northern stations, the nitrate and SRP concentrations showed a sharp cline spanning the chlorophyll peak. At St. 3, the slope was less steep than that at the other two stations, and the nitrate concentrations were < 1 μM at the SCM. A primary nitrite maximum (PNM) was observed around the SCM at all three stations, which is typical of the eastern Indian Ocean, although its depth and magnitude varied from station to station. At St. 2, the PNM occurred approximately 10 m below the SCM, and its magnitude was the largest of the three stations, reaching 1.8 μM. The PNM at St. 3 appeared at >20 m below the SCM, whereas that at St. 4 nearly coincided with the SCM.

At the three southern stations, nutrient concentrations were vertically uniform across the sampling range, likely reflecting strong mixing in the upper water column (Fig. 1). Nitrate concentrations were at or near detection limits throughout the sampling range (typically <0.2 μM). The SRP concentration was higher than that of the two nitrogen species, suggesting potential nitrogen limitation across the sampling range.

4. Discussion

4.1. Characterizing the SCM observed in the eastern Indian Ocean

We successfully obtained seawater samples at approximately 3-m intervals with minimal changes in the water column status by slowly winding up water samplers without halting the winch. Because we needed to determine a sampling range based on the chlorophyll profile obtained during the downcast, the SCM could have been missed if the vertical movement of the water mass was highly dynamic. As an example of such a mismatch, the SCM appeared near the top of the sampling range at St. 3. To minimize the risk of such a mismatch, the sampling range should be as wide as possible, while simultaneously using as many water samplers as possible. Although observations using *in situ* sensors can reveal distributions of phytoplankton biomass and photosynthetic parameters at various spatial resolutions spanning from centimeter- (Doubell et al., 2009; Priyadarshi et al., 2019) to meter-level (Kerkar et al., 2020; Wang et al., 2024), the number of available parameters is limited, and their precision can be affected by water motion. In contrast, high-frequency sampling with water samplers enables multiparameter analysis at each depth, though the spatial resolution is limited by the length of the samplers, which is typically >1 m. The sampling interval used in this study (3 m) was close to the theoretical minimum and smaller than those reported in previous studies (van den Engh et al., 2017; Sato et al., 2022b).

In this study, conducted in the eastern Indian Ocean during the late boreal summer, a distinct SCM was observed at all stations except St. 8 (Fig. 1; Table 1). These SCM largely coincided with the top of the seasonal pycnocline, except at St. 9, where no seasonal pycnocline was observed within the upper 200 m, suggesting the importance of physical accumulation for the SCM formation and maintenance. Phytoplankton distribution has been intensively surveyed in the eastern Indian Ocean, particularly in the Bay of Bengal (Murty et al., 2000; Liu et al., 2011; Li et al., 2012a, b; Yuan et al., 2021), indicating that SCM occurrence around the pycnocline is ubiquitous in this area. Time-series observations during the summer monsoon season (Prasanth et al., 2023) revealed that the SCM in the Bay of Bengal occurs within the barrier layer and euphotic zone. Although the formation and maintenance of the chlorophyll *a* peak unaccompanied by a pycnocline at St. 9 is unclear from the present observations, faint solar irradiance (<10 μmol photons m^{-2} s^{-1}), approximately one tenth of E_k (Fig. 2) in this layer, suggests that it was difficult for phytoplankton to maintain growth. This may be a remnant of the phytoplankton assemblage that grew in the upper layers. The larger chlorophyll *a* peak at approximately 150 m at St. 7 (Fig. 1) can be explained similarly.

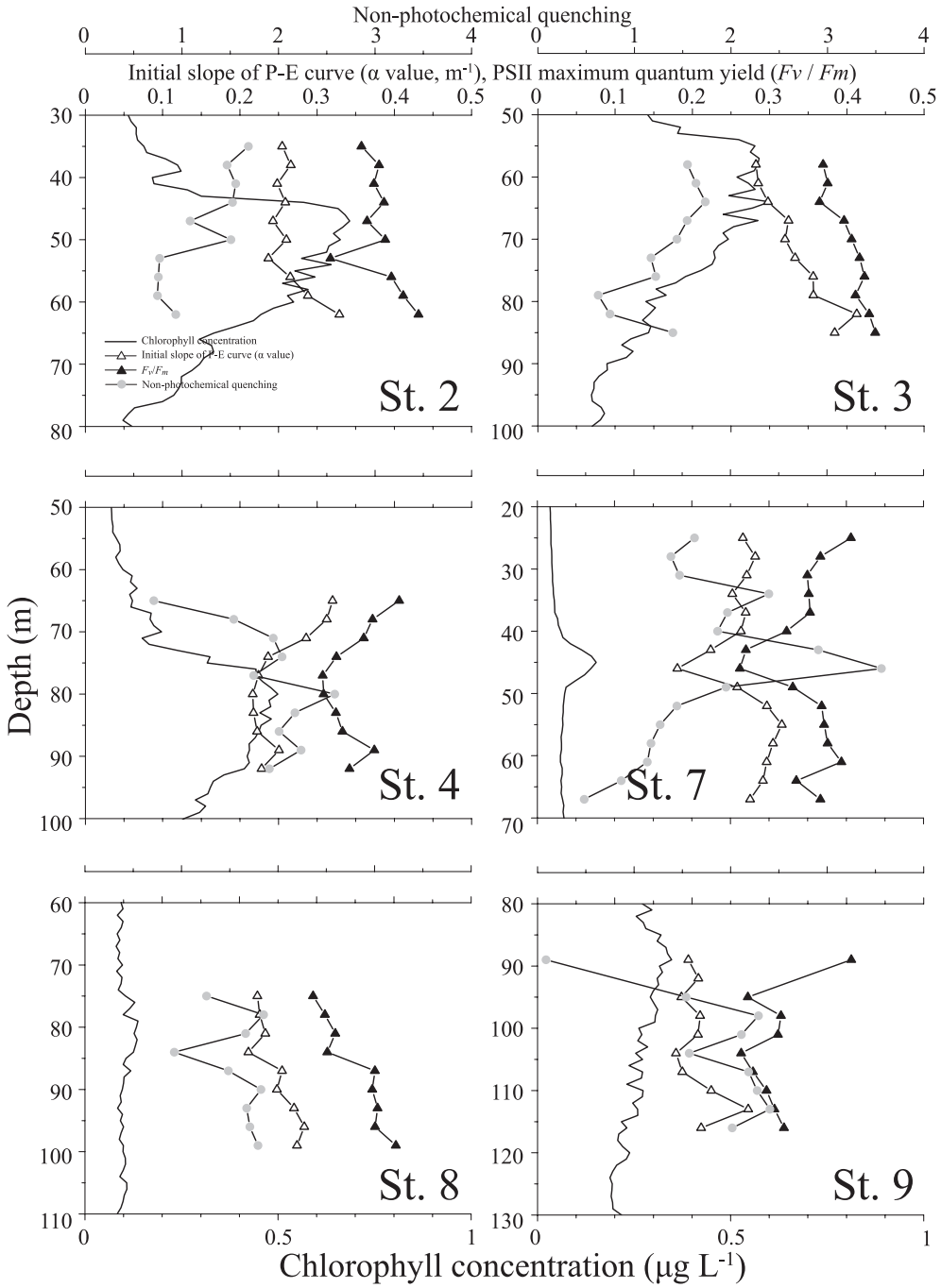

Fig. 3. Vertical profiles of the initial slope of the P-E curve (α-value, blank triangles, m^{-1}), the maximum quantum yield of photosystem II (PSII) (F_v/F_m, solid triangles), and non-photochemical quenching (NPQ_{NSV}, grey circles) around the SCM, estimated using STAF, along with those of chlorophyll concentration (solid line, μg L^{-1}).

4.2. General vertical trends in photosynthetic parameters in the eastern Indian Ocean

At all the stations except at St. 2, the fluorometry was initiated within 1 h of sample retrieval and completed within 5 h (Table 1). Because they were kept in the dark from the moment the seawater samples were collected into Niskin samplers, the dark acclimation period was at least approximately 20 min. We acknowledge that measurements obtained after extended dark acclimation do not reflect instantaneous *in situ* physiological states. Instead, our approach aimed to assess photosynthetic properties under fully relaxed conditions, allowing for standardized comparisons across depths. Although similar acclimation periods have been used in previous studies, laboratory studies have shown that they are insufficient to negate the effects of light history (Bruyant et al., 2005; Mella-Flores et al., 2012; From et al., 2014). However, the F_v/F_m ratio of *Prochlorococcus* cultured under lower light (~1.5 times E_k) showed no significant diel variation after 15 minutes of dark acclimation (Zinser et al., 2009). Although there have been scarce data on how long it takes for phytoplankton acclimated to dim light, like those in the current study, to fully recover from the effect of light history, F_v/F_m ratios of algal cultures incubated under low irradiance (<100 μmol photons m^{-2} s^{-1}) showed almost no effect of light history after 30 min of dark acclimation (From et al., 2014). Considering that the ambient irradiance level is similar to or lower than E_k (Fig. 2), 20 min of dark

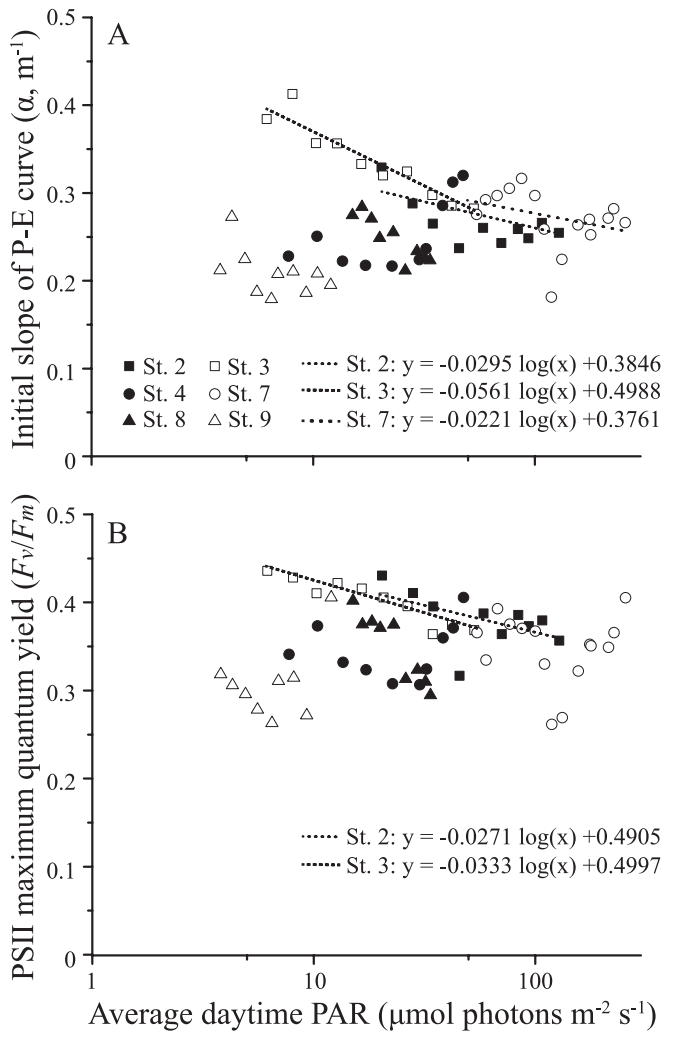

Fig. 4. Scatter plots of the initial slope of the P-E curve (α-value, A, m^{-1}), quantum yield of PSII (F_v/F_m, B) against the estimated 8-day-averaged PAR irradiance during daytime around the SCM for each station (solid square, St. 2; blank square, St. 3; solid circle, St. 4; blank circle, St. 7; solid triangle, St. 8; blank triangle, St. 9). The regression lines for each photosynthetic parameter plotted against the log of the PAR irradiance are shown as dashed lines, along with the formula.

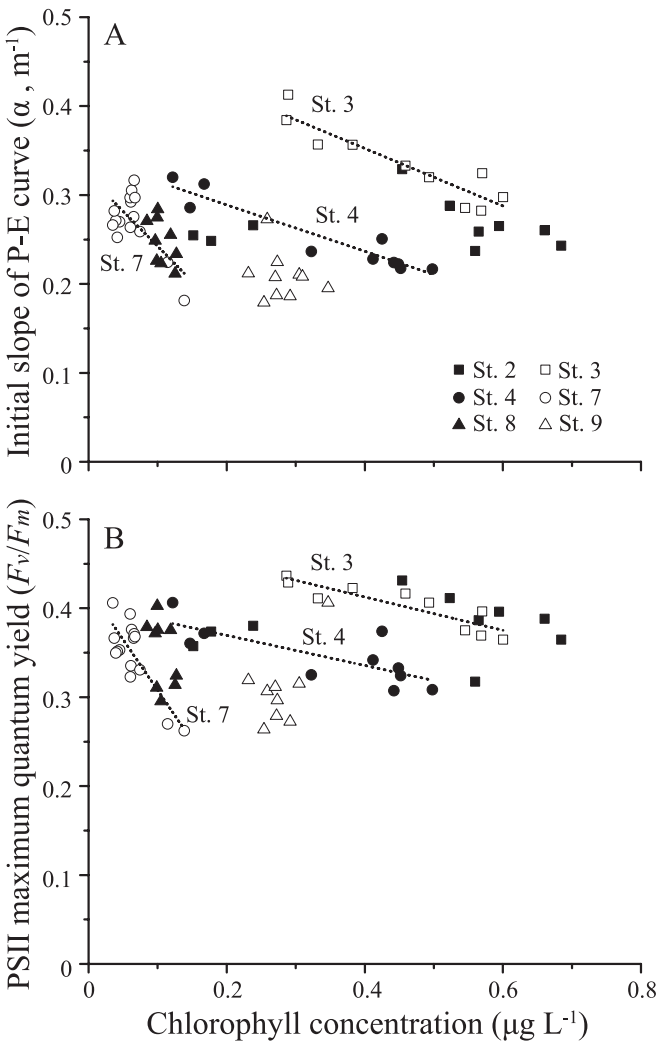

Fig. 5. Scatter plots of the initial slope of the P-E curve (α-value, A, m^{-1}), quantum yield of PSII (F_v/F_m, B) against chlorophyll concentration around the SCM for each station (solid square, St. 2; blank square, St. 3; solid circle, St. 4; blank circle, St. 7; solid triangle, St. 8; blank triangle, St. 9). Regression lines are shown only when their slopes were significantly different from zero ($P < 0.05$).

acclimation can negate at least some of the effects of light history on fluorometry. Prolonged darkness can affect the physiological status of phytoplankton, likely due to trace metal contamination or bottle containment. A dark acclimation period of 20 min to 5 h is considered an effective tradeoff between recovery from light stress and bottle effects. Longer dark periods at St. 2 (Table 1) may have negatively affected phytoplankton physiological status.

In this study, fluorometry was conducted at different local times from station to station, and the samples were measured over a total of approximately 3 h (Table 1), starting with the shallowest depths and progressing to the deepest, or *vice versa*. These differences in measurement timing may have caused artifactual variations in photosynthetic parameters within and among stations, given the distinct diel variations in phytoplankton photosynthetic parameters (Long et al., 1994). However, F_v/F_m ratios against ambient daytime PAR irradiance were scattered around nearly the same curve, except for those near the SCM and at St. 9 (Fig. 4B), despite differences in local time of measurement among the stations (Table 1). Whereas the suppressed F_v/F_m ratio at St. 9 may have reflected a decrease in F_v/F_m from sunrise to midday, which is usually observed (Behrenfeld and Kolber, 1999), this suppression was not observed at the other stations where fluorometry was conducted around noon (Sts. 4 and 7). A lack of a midday decrease in F_v/F_m was observed for both subsurface natural assemblages in the South China Sea (below 40 m) (Xie et al., 2018) and a high-light-adapted *Prochlorococcus* culture incubated at an irradiance of approximately 1.5 times E_k (Zinser et al., 2009). Thus, it is likely that diel variations in photosynthetic parameters are diminished under the light level, similar with or lower than E_k, experienced in the subsurface waters (Fig. 2). Therefore, in the present study, difference in the sampling time is unlikely to have accounted for the vertical variations in F_v/F_m.

The decrease in E_k values with depth at the four northern stations (Fig. 2) supports photoacclimation and photoadaptation in subsurface waters, as previously reported (Moore et al. 2006; Yuan et al. 2019). The slope of the natural logarithm of E_k values against depth was smaller (in absolute value) than that of the ambient PAR irradiance at all four stations, where a significant decrease in E_k with depth was observed (Table 3). However, the difference between the two slopes was significant only for Sts. 2 and 7 ($P < 0.05$ and $P < 0.001$, respectively; *F*-test). The less steep slope of E_k than that of ambient PAR suggests that the potential photophysiological capability of the phytoplankton assemblages to adjust to low-light conditions was not sufficient to fully compensate for natural light attenuation at these two stations.

Table 4
Slopes of regression lines of initial slope of photosynthesis, maximum quantum of photosystem II, and non-photochemical quenching on chlorophyll *a* concentration at Stations 3, 4, and 7. All the values are shown with 95% confidence intervals.

	α value vs. chlorophyll			F_v/F_m vs. chlorophyll			NPQ vs. chlorophyll		
St. 3	−0.323	±	0.048	−0.187	±	0.033	2.398	±	0.666
St. 4	−0.261	±	0.032	−0.169	±	0.051	2.534	±	0.839
St. 7	−0.788	±	0.247	−1.139	±	0.230	17.69	±	5.97

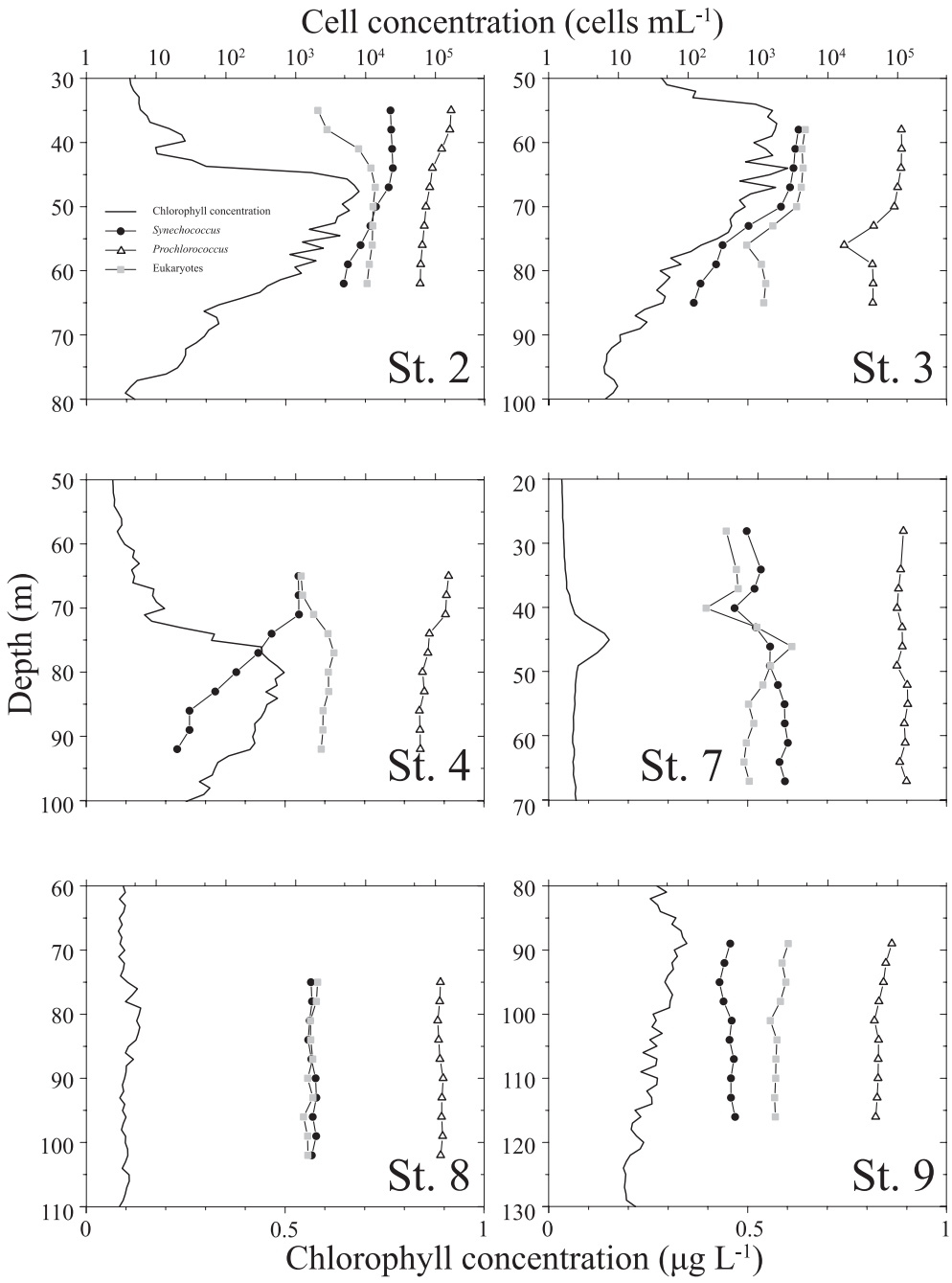

Fig. 6. Vertical profiles of the cell concentrations (cells mL^{-1}) of *Synechococcus* (solid circles), *Prochlorococcus* (blank triangles), and eukaryotic phytoplankton (grey squares) around the SCM, as determined by flow cytometry, together with chlorophyll concentration (solid line, μg L^{-1}).

The relatively constant E_k values at Sts. 8 and 9 were consistent with a relatively constant density (Fig. 1), suggesting that the upper water column was well-mixed on a timescale shorter than that of photoacclimation. In contrast, the distinct gradient in the E_k values at St. 7, despite the relatively small density gradient in and slight seasonal pycnocline, suggests relatively weak mixing, which may have contributed to phytoplankton accumulation in the subsurface layer. The potential light limitation suggested by the relatively high E_k values agrees with our previous report from the same area, in which light was the primary limiting factor for phytoplankton growth in the SCM (Sato et al.,

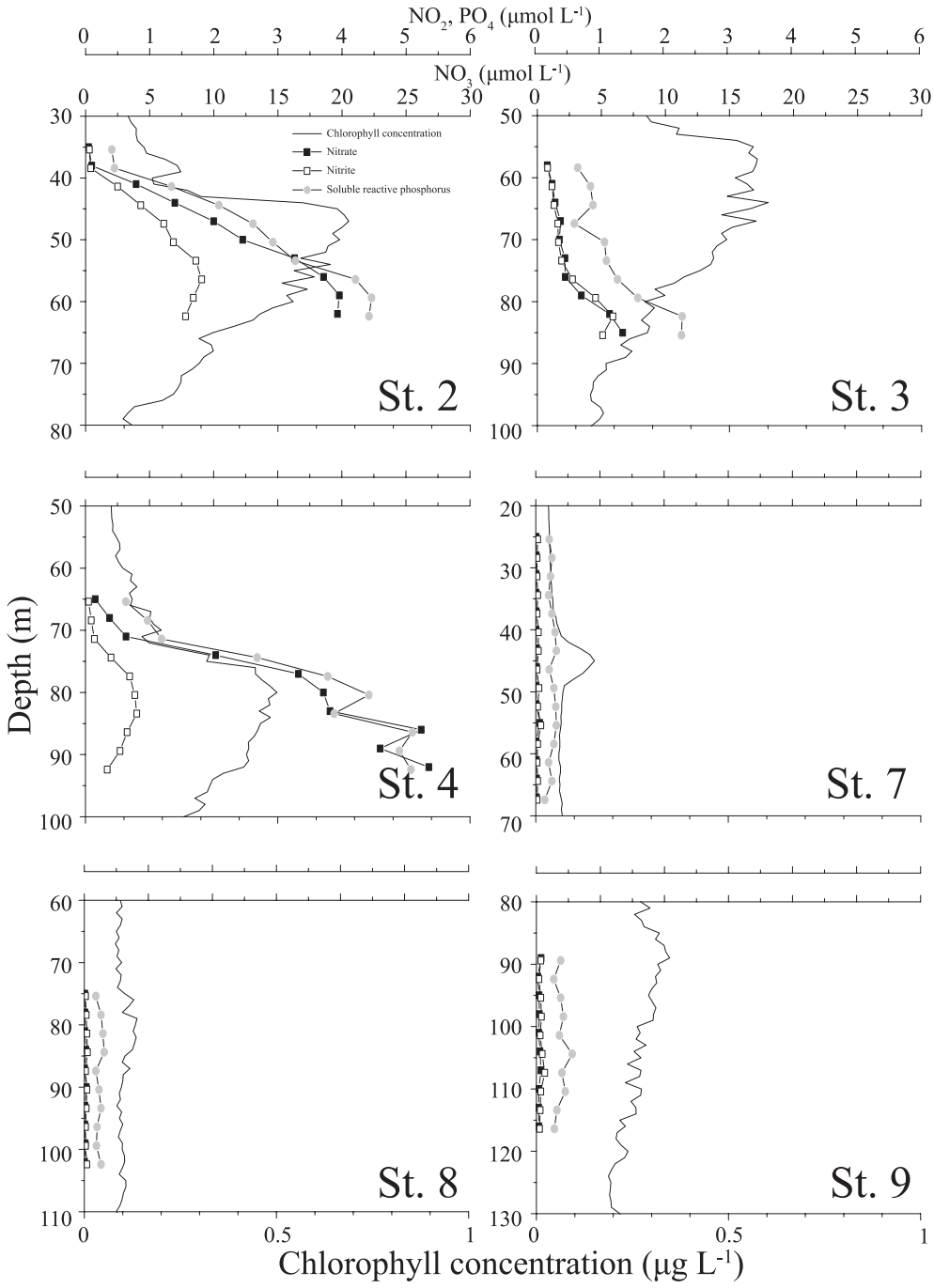

Fig. 7. Vertical profiles of nitrate (solid squares), nitrite (blank squares), and soluble reactive phosphorus (grey circles) concentrations around the SCM, together with chlorophyll concentration (solid line, μg L^{-1}).

2022b).

The cellular chlorophyll content of *Prochlorococcus* and *Synechococcus*, indexed by cellular red fluorescence, increased with depth (Fig. S4), which likely accounts for acclimation and adaptation to dim environments. Notably, the cellular chlorophyll fluorescence of the eukaryotes decreased with increasing depth at all four stations (Fig. S4). However, the cellular forward light scatter of eukaryotes decreased with depth, except at St. 3 (Fig. S5), suggesting that the miniaturization of their mean cell size may compensate for the decrease in cellular chlorophyll content. In addition to the dark acclimation and adaptation of each phytoplankton population, vertical variations in the composition of phytoplankton communities (Fig. 6) may have contributed to the changes in E_k values, which can show intra- and interspecific variations in both prokaryotic and eukaryotic algae (Moore et al., 1995; MacIntyre et al., 2002; Six et al., 2021). At this point, however, it would be more reasonable to select species and ecotypes adapted to the ambient light environment and the resultant variations in phytoplankton community composition would form the vertical profiles of E_k.

Other photosynthetic parameters derived from STAF, α and NPQ_{NSV}, showed similar vertical variations across the SCM among the different stations, particularly at Sts. 3, 4, and 7 (Figs. 3, 4, and 5). Although these parameters are not strictly independent of each other (see Materials and Methods, Schuback et al., 2015; Wei et al., 2019), their similarities suggest that photosynthesis is controlled by similar mechanisms at these stations. Generally, the α values and F_v/F_m increased with depth, while NPQ_{NSV} decreased. Similar vertical trends have been confirmed for α

values (Cullen et al., 1992; Sathyendranath et al., 1996; Yoshikawa and Furuya, 2008), F_v/F_m (Boyd and Abraham, 2001; Yuan et al., 2019; Kerkar et al., 2020), and NPQ_{NSV} (Raateoja et al., 2009; Wang et al., 2024). These overall trends are likely driven primarily by the alleviation of photoinhibition and increased nutrient availability with depth (Kerkar et al., 2020). This suggests that the effects of photoinhibition were not completely eliminated from the subsurface phytoplankton assemblages even after > 20 min of dark acclimation.

Photosynthetic parameters are affected not only by phytoplankton physiological status but also by species composition. For example, F_v/F_m and σ_{PSII} of *Synechococcus* are generally lower than those of *Prochlorococcus* or eukaryotic phytoplankton under similar conditions (Sugget et al., 2009; Mella-Flores et al., 2012), owing to the involvement of phycobilins, which cannot be effectively excited by blue light used in this study. These interspecific variations may partly account for the increase in F_v/F_m with depth, taking into account that the relative contribution of *Synechococcus* decreased with depth at Sts. 2, 3, and 4 (Fig. 6). In eukaryotes, the F_v/F_m ratios of diatoms are generally higher than those of picoeukaryotes (Suggett et al., 2009). Although the community composition of eukaryotic phytoplankton was not analyzed in the current study, eukaryotic phytoplankton in the subsurface waters of the eastern Indian Ocean are generally dominated by pico-sized eukaryotes (Guo et al., 2023), suggesting that the effect of eukaryotic community composition on photosynthetic parameters was not significant. In addition to the shift in community composition, the presence of phaeophytin, a chlorophyll degradant, is known to lower F_v/F_m without affecting σ_{PSII} (Fuchs et al., 2002). However, the observation that F_v/F_m increased with depth below the SCM suggests that the effect of phaeophytin on F_v/F_m was minor, given that the ratio of phaeophytin to chlorophyll generally increases with depth below the SCM.

Because the α values were obtained by fluorometry, it is difficult to directly compare their absolute values with those of previous studies, most of which were derived from isotope incorporation experiments. Here, we compared the F_v/F_m values obtained in this study with those obtained from subsurface waters in other studies. *The* F_v/F_m values of ~0.4 found off the SCM peak in the current study were similar to those observed between 15 °N and 10 °S in the eastern Indian Ocean in boreal late spring (Wang et al., 2024). Thus, these are typical values for F_v/F_m in the subsurface layers of stratified areas of the eastern Indian Ocean. Similar values were observed in the subsurface waters of the subtropical front of the Southern Ocean (Kerkar et al., 2020) and Drake Passage (Hopkinson et al., 2007), but were lower than those in the North Pacific Subtropical Gyre (Vaillacourt et al., 2003) and Southern California Bight (Hopkinson and Barbeau, 2008). The F_v/F_m values found around the SCM peak (0.26–0.36, Fig. 3) are within ranges similar to those found in the subsurface waters of the Bay of Bengal (Wei et al., 2019), Antarctic Circumpolar Current (Hopkinson et al., 2007), and Antarctic Polar Front (Kerkar et al., 2020).

4.3. Local variations in photosynthetic parameters around the SCM

This study is the first to discuss a reduced F_v/F_m ratio around the SCM peak (Fig. 3). Generally, the F_v/F_m value increases with depth in natural phytoplankton assemblages in open oceans (Yuan et al., 2019; Kerkar et al., 2020), which is likely due to the alleviation of photoinhibition and/or nutrient limitation. Because a depressed F_v/F_m was observed at 10–20 m around the SCM (Fig. 3), this depression could have been overlooked if the conventional sampling method was employed at typical intervals of 10–25 m. Lower F_v/F_m values around the SCM were observed within cyclonic eddies in the subtropical North Pacific (Fig. 4b in Vaillancourt et al., 2003) and the subtropical front of the Southern Ocean (Fig. 6a in Kerkar et al., 2020), although the authors did not mention this phenomenon. In a semi-continuous survey covering the eastern Indian Ocean, the decrease in F_v/F_m values around the SCM was unclear, except at the equator (Fig. 6 in Wang et al., 2024), and was not specifically noted.

Based on the discussion in the previous section, it is unlikely that local variations in photosynthetic parameters around the SCM at Sts. 3, 4, and 7 can be attributed to photoinhibition, limitation by macronutrients, and chlorophyll degradants, although these factors, particularly the former two, can largely explain their variation on a larger vertical scale. Although the positive correlation of the α and F_v/F_m values with nitrogen nutrients (Fig. 8) at St. 3 suggests that the depression of these values was caused by macronutrient deficiency, it should be considered that the sampling range only covered depths lower than the SCM peak at this station (Fig. 1). In other words, negative correlation of the α and F_v/F_m values with chlorophyll at St. 3 (Fig. 5) are likely explained by alleviation from macronutrient limitation below the SCM.

However, the negative correlation between the α and F_v/F_m values and chlorophyll at Sts. 4 and 7 (Fig. 5) cannot be similarly explained. One possible cause for the depression in the α and F_v/F_m around the SCM concomitant with the increase in NPQ_{NSV} is a vertical variation in the phytoplankton community composition (Sugget et al., 2009), as mentioned in section 4.2. However, the relatively constant contributions of *Prochlorococcus* and eukaryotes with a minor contribution of *Synechococcus* within the SCM at St. 4 (Fig. 6) suggested that local variations in photosynthetic parameters were unlikely to be caused by interspecific variations. In contrast, the relatively high contributions of eukaryotic

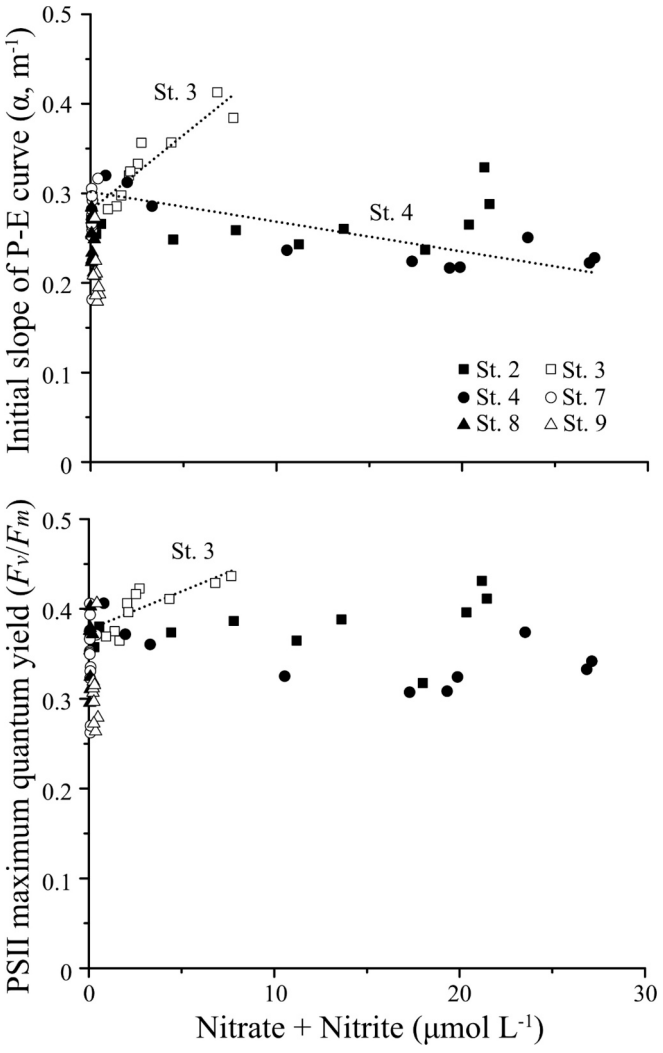

Fig. 8. Scatter plots of the photosynthesis-irradiance curve (α-value, A), quantum yield of photosystem II (F_v/F_m, B) against the sum of nitrate and nitrite concentrations around the SCM for each station. Regression lines are shown only when their slopes were significantly different from zero ($P < 0.05$). Symbols for each station are the same as in Fig. 4.

phytoplankton at the SCM of St. 7 (Fig. 6) may partly account for the variations in photosynthetic parameters at this station. Because interspecific variations in photosynthetic parameters are observed even among eukaryotes (Kruskopf and Flynn, 2006; Sugget et al., 2009), more detailed analysis of phytoplankton community structure is required, which was not achieved by flow cytometry.

Another possible explanation for the local variations in photosynthetic parameters around the SCM is physiological stress caused by iron deficiency. It is widely known that physiological stress on phytoplankton due to iron deficiency results in changes in their photosynthetic parameters, particularly a decrease in F_v/F_m for both laboratory cultures (Greene et al., 1991) and natural assemblages (Kolber et al., 1994; Suzuki et al., 2002). A concomitant increase in the NPQ_{NSV} around the SCM at Sts. 4 and 7 (Fig. 3) is also indicative of photophysiological stress induced by iron deficiency (Ryan-Keogh et al., 2023). Considering the nutrient-like vertical profile of dissolved iron in the open ocean, it may be unreasonable that photosynthetic systems around the SCM are more severely iron limited than those in the adjacent waters. However, many observations have reported subsurface dissolved iron minima that largely coincide with the SCM in subtropical open waters (Bruland et al., 1994; Sedwick et al., 2005; Hawco et al., 2021). These subsurface minima of dissolved iron are caused by the increased demand for iron by chlorophyll synthesis under low-light conditions (Raven, 1988; Sunda and Huntsman, 1997), as evidenced by the accumulation of chlorophyll at the SCM. Light-iron colimitation on phytoplankton growth around the SCM has been experimentally verified in subtropical waters (Hogle et al., 2018; Hawco et al., 2021), including the Indian Ocean (Sato et al., 2022b; Sun et al., 2024). Stoichiometric analyses also suggest a potential relative deficiency of iron compared with other biogenic elements in the eastern Indian Ocean (Thi Dieu Vu and Sohrin, 2013; Twining et al., 2019). This is consistent with the hypothesis that subsurface variations in photosynthetic parameters in the subtropical Indian Ocean are associated with iron deficiency.

However, the responses of photosynthetic parameters, particularly F_v/F_m, to iron deficiency are not straightforward in marine phytoplankton (Behrenfeld et al., 2006b; Behrenfeld and Milligan, 2013), which are influenced by community composition, availability of macronutrients, and diel variations. Whether the F_v/F_m signature characteristic of iron-limited phytoplankton assemblages at the surface is observed for subsurface iron-limited assemblages remains unclear. In the Southern California Bight region, where subsurface phytoplankton assemblages are co-limited by iron and light, the F_v/F_m values of unamended subsurface phytoplankton assemblages are relatively high (~0.5); however, F_v/F_m is enhanced by either iron enrichment or elevated light irradiation (Hopkinson and Barbeau, 2008). In the current study, stringent trace-metal-clean techniques were not applied, and iron concentrations were not measured in the samples obtained during fine-scale SCM sampling. Thus, it is impossible to directly evaluate the physiological stress on phytoplankton assemblages and the proposed light-iron co-limitation remains a working hypothesis. Moreover, intraspecific variation in photosynthetic parameters (Kruskopf and Flynn, 2006; Sugget et al., 2009), which may account for the variations around the SCM, was not evaluated in this study due to methodological limitations. Thus, manipulation experiments using stringent trace-metal-clean techniques, fluorometric approaches and analyses of phytoplankton community composition will help reveal the mechanisms controlling the photosynthetic parameters of subsurface phytoplankton assemblages in the eastern Indian Ocean.

5. Conclusions

From high-resolution vertical profiles of photosynthetic parameters measured in the eastern Indian Ocean, we found reductions in α and F_v/F_m values, and an increase in NPQ_{NSV}, around the SCM of the subtropical stratified waters. These fine-scale variations in photosynthetic parameters likely result in a significant reduction in potential carbon fixation around the SCM, which is likely ignored if the conventional sampling method at ~10-m intervals is employed. Typically, biogeochemical models have assumed that carbon-specific photosynthetic rates in the open ocean decrease with depth, in response to light attenuation. However, the present results suggest the possibility of an additional depression in photosynthesis around the SCM. This challenges the validity of current evaluations of ocean productivity in subsurface waters. It is essential to understand how far this depression extends horizontally and vertically, and what causes it, for refined estimates of global ocean productivity. Photoinhibition or macronutrient (nitrogen) deficiency, which is a likely cause of the surface depression of F_v/F_m in the surface of subtropical waters, cannot account for the restrained potential photosynthesis around the SCM. In addition to variations in the phytoplankton community composition, iron deficiency is a possible cause of local variations in photosynthetic parameters around the SCM. However, a direct examination of the effects of iron bioavailability on photosynthetic parameters in subsurface waters is required. The horizontal and vertical dimensions of potential iron limitations in subsurface waters worldwide, and their impacts on global primary productivity, should be assessed using a wide range of techniques, including high-resolution sampling, fluorometric assessment of potential photosynthesis, direct measurement of carbon fixation, and enrichment experiments. The potential targeted areas will include subtropical North and South Pacific and Indian Ocean, where potential iron deficiency in subsurface phytoplankton assemblages has been suggested. It will contribute to prediction of interactive effects of subsurface ecosystems and global climate changes.

CRediT authorship contribution statement

Mitsuhide Sato: Writing – original draft, Visualization, Investigation, Funding acquisition, Conceptualization. **Takako Masuda:** Writing – original draft, Investigation, Funding acquisition. **Yoshiko Kondo:** Writing – review & editing, Funding acquisition. **Takuya Sato:** Writing – review & editing, Investigation, Funding acquisition. **Hiroaki Saito:** Writing – review & editing, Investigation.

Declaration of competing interest

The authors declare that they have no known competing financial interests or personal relationships that could have appeared to influence the work reported in this paper.

Acknowledgements

We thank the captain, crew, and scientists on board the Hakuho-maru KH-24-3 cruise for their help with observations and sample collection. This study was supported by Cooperative Research Program of Atmosphere and Ocean Research Institute, The University of Tokyo (R/V Hakuho-Maru KH-24-3 cruise, JURCAOSSH24-08). Maiko Ito technically supported the operation of the nutrient autoanalyzer.

Funding

This work was supported by JSPS grants 23K26994, 24K07202, and 24KK0193, and by JST grants PRESTO JPMJPR23G5 and JPMJPR23GA.

Appendix A. Supplementary data

Supplementary data to this article can be found online at https://doi.org/10.1016/j.pocean.2026.103810.

Data availability

Data will be made available on request.

References

Anderson, G.C., 1969. Subsurface chlorophyll maximum in the northeast Pacific Ocean. Limnol. Oceanogr. 14, 386–391.

Argo, 2000. Argo float data and metadata from Global Data Assembly Centre (Argo GDAC). SEANOE. https://doi.org/10.17882/42182.

Behrenfeld, M.J., Kolber, Z.S., 1999. Widespread iron limitation of phytoplankton in the South Pacific Ocean. Science 283, 840–843.

Behrenfeld, M.J., O'Malley, R.T., Siegel, D.A., McClain, C.R., Sarmiento, J.L., Feldman, G.C., Milligan, A.J., Falkowski, P.G., Letelier, R.M., Boss, E.S., 2006a. Climate-driven trends in contemporary ocean productivity. Nature 444, 752–755.

Behrenfeld, M.J., Worthington, K., Sherrell, R.M., Chavez, F.P., Strutton, P., McPhaden, M., Shea, D.M., 2006b. Controls on tropical Pacific Ocean productivity revealed through nutrient stress diagnostics. Nature 442, 1025–1028.

Behrenfeld, M.J., Milligan, A.J., 2013. Photophysiological expressions of iron stress in phytoplankton. Ann. Rev. Mar. Sci. 5, 217–246.

Bibby, T.S., Gorbunov, M.Y., Wyman, K.W., Falkowski, P.G., 2008. Photosynthetic community responses to upwelling in mesoscale eddies in the subtropical North Atlantic and Pacific Oceans. Deep Sea Res. Part II 55, 1310–1320.

Boatman, T.G., Geider, R.J., Oxborough, K., 2019. Improving the accuracy of single turnover active fluorometry (STAF) for the estimation of phytoplankton primary productivity (PhytoPP). Front. Mar. Sci. 6. https://doi.org/10.3389/fmars.2019.00319.

Boyd, P.W., Abraham, E.R., 2001. Iron-mediated changes in phytoplankton photosynthetic competence during SOIREE. Deep-Sea Res. Part II-Topical Stud. Oceanography 48, 2529–2550.

Brittain, G.C., Chen, Y.Q., Martinez, E., Tang, V.A., Renner, T.M., Langlois, M.-A., Gulnik, S., 2019. A novel semiconductor-based flow cytometer with enhanced light-scatter sensitivity for the analysis of biological nanoparticles. Sci. Rep. 9, 16039.

Bruland, K.W., Orians, K.J., Cowen, J.P., 1994. Reactive trace metals in the stratified central North Pacific. Geochim. Cosmochim. Acta 58, 3171–3182.

Bruyant, F., Babin, M., Genty, B., Prasil, O., Behrenfeld, M.J., Claustre, H., Bricaud, A., Garczarek, L., Holtzendorff, J., Koblizek, M., Dousova, H., Partensky, F., 2005. Diel variations in the photosynthetic parameters of *Prochlorococcus* strain PCC 9511: Combined effects of light and cell cycle. Limnol. Oceanogr. 50, 850–863.

Cheah, W., McMinn, A., Griffiths, F.B., Westwood, K.J., Wright, S.W., Clementson, L.A., 2013. Response of phytoplankton photophysiology to varying environmental conditions in the Sub-Antarctic and Polar Frontal Zone. PLoS One 8, e72165.

Chen, Y.L.L., 2005. Spatial and seasonal variations of nitrate-based new production and primary production in the South China Sea. Deep Sea Res. Part 1 Oceanogr. Res. Pap. 52, 319–340.

Cornec, M., Claustre, H., Mignot, A., Guidi, L., Lacour, L., Poteau, A., D'Ortenzio, F., Gentili, B., Schmechtig, C., 2021. Deep chlorophyll maxima in the global ocean: occurrences, drivers and characteristics. Global Biogeochem. Cycles 35, e2020GB006759.

Cullen, J.J., Lewis, M.R., Davis, C.O., Barber, R.T., 1992. Photosynthetic characteristics and estimated growth rates indicate grazing is the proximate control of primary production in the equatorial Pacific. J. Geophys. Res. Oceans 97, 639–654.

DiTullio, G.R., Geesey, M.E., Jones, D.R., Daly, K.L., Campbell, L., Smith Jr, W.O., 2003. Phytoplankton assemblage structure and primary productivity along 170°W in the South Pacific Ocean. Mar. Ecol. Prog. Ser. 255, 55–80.

Doubell, M.J., Yamazaki, H., Li, H., Kokubu, Y., 2009. An advanced laser-based fluorescence microstructure profiler (TurboMAP-L) for measuring bio-physical coupling in aquatic systems. J. Plankton Res. 31, 1441–1452.

From, N., Richardson, K., Mousing, E.A., Jensen, P.E., 2014. Removing the light history signal from normalized variable fluorescence (Fv/Fm) measurements on marine phytoplankton. Limnol. Oceanogr. Methods 12, 776–783.

Fuchs, E., Zimmerman, R.C., Jaffe, J.S., 2002. The effect of elevated levels of phaeophytin in natural water on variable fluorescence measured from phytoplankton. J. Plankton Res. 24, 1221–1229.

Greene, R.M., Geider, R.J., Falkowski, P.G., 1991. Effect of iron limitation on photosynthesis in a marine diatom. Limnol. Oceanogr. 36, 1772–1782.

Guo, S., Wang, F., Liang, J., Zhang, K., Sun, X., 2023. Phytoplankton carbon biomass: Insights from the eastern Indian Ocean. *Deep-Sea Research Part I: Oceanographic Research Papers*, 202.

Hawco, N.J., Barone, B., Church, M.J., Babcock-Adams, L., Repeta, D.J., Wear, E.K., Foreman, R.K., Björkman, K.M., Bent, S., Van Mooy, B.A.S., Sheyn, U., DeLong, E.F., Acker, M., Kelly, R.L., Nelson, A., Ranieri, J., Clemente, T.M., Karl, D.M., John, S.G., 2021. Iron depletion in the deep chlorophyll maximum: mesoscale eddies as natural iron fertilization experiments. Global Biogeochem. Cycles 35, e2021GB007112.

Hogle, S.L., Dupont, C.L., Hopkinson, B.M., King, A.L., Buck, K.N., Roe, K.L., Stuart, R.K., Allen, A.E., Mann, E.L., Johnson, Z.I., Barbeau, K.A., 2018. Pervasive iron limitation at subsurface chlorophyll maxima of the California Current. Proc. Natl. Acad. Sci., USA 115, 13300–13305.

Hopkinson, B.M., Barbeau, K.A., 2008. Interactive influences of iron and light limitation on phytoplankton at subsurface chlorophyll maxima in the eastern North Pacific. Limnol. Oceanogr. 53, 1303–1318.

Hopkinson, B.M., Mitchell, B.G., Reynolds, R.A., Wang, H., Selph, K.E., Measures, C.I., Hewes, C.D., Holm-Hansen, O., Barbeau, K.A., 2007. Iron limitation across chlorophyll gradients in the southern Drake Passage: phytoplankton responses to iron addition and photosynthetic indicators of iron stress. Limnol. Oceanogr. 52, 2540–2554.

Kerkar, A.U., Tripathy, S.C., Minu, P., Baranval, N., Sabu, P., Patra, S., Mishra, R.K., Sarkar, A., 2020. Variability in primary productivity and bio-optical properties in the Indian sector of the Southern Ocean during an austral summer. Polar Biol. 43, 1469–1492.

Kolber, Z.S., Barber, R.T., Coale, K.H., Fitzwateri, S.E., Greene, R.M., Johnson, K.S., Lindley, S., Falkowski, P.G., 1994. Iron limitation of phytoplankton photosynthesis in the equatorial Pacific Ocean. Nature 371, 145–149.

Kolber, Z.S., Prášil, O., Falkowski, P.G., 1998. Measurements of variable chlorophyll fluorescence using fast repetition rate techniques: defining methodology and experimental protocols. Biochim. Biophys. Acta (BBA) - Bioenergetics, 1367, 88-106.

Kruskopf, M., Flynn, K.J., 2006. Chlorophyll content and fluorescence responses cannot be used to gauge reliably phytoplankton biomass, nutrient status or growth rate. New Phytol. 169, 525–536.

Letelier, R.M., Karl, D.M., Abbott, M.R., Bidigare, R.R., 2004. Light driven seasonal patterns of chlorophyll and nitrate in the lower euphotic zone of the North Pacific Subtropical Gyre. Limnol. Oceanogr. 49, 508–519.

Li, G., Ke, Z., Lin, Q., Ni, G., Shen, P., Liu, H., Yin, J., Li, K., Huang, L., Tan, Y., 2012a. Longitudinal patterns of spring-intermonsoon phytoplankton biomass, species compositions and size structure in the Bay of Bengal. Acta Oceanol. Sin. 31, 121–128.

Li, G., Lin, Q., Ni, G., Shen, P., Fan, Y., Huang, L., Tan, Y., 2012b. Vertical patterns of early summer chlorophyll *a* concentration in the Indian Ocean with special reference to the variation of deep chlorophyll maximum. J. Mar. Sci. 2012, 801248.

Liu, H., Ke, Z., Song, X., Tan, Y., Huang, L., Ln, Q., 2011. Primary production in the Bay of Bengal during spring intermonsoon period. Acta Ecol. Sin. 31, 7007–7012.

Long, S.P., Humphries, S., Falkowski, P.G., 1994. Photoinhibition of photosynthesis in nature. Annu. Rev. Plant Biol. 45, 633–662.

MacIntyre, H.L., Kana, T.M., Anning, T., Geider, R.J., 2002. Photoacclimation of photosynthesis irradiance response curves and photosynthetic pigments in microalgae and cyanobacteria. J. Phycol. 38, 17–38.

Marañón, E., Van Wambeke, F., Uitz, J., Boss, E.S., Dimier, C., Dinasquet, J., Engel, A., Haëntjens, N., Pérez-Lorenzo, M., Taillandier, V., Zäncker, B., 2021. Deep maxima of phytoplankton biomass, primary production and bacterial production in the Mediterranean Sea. Biogeosciences 18, 1749–1767.

Masuda, T., Furuya, K., Kohashi, N., Sato, M., Takeda, S., Uchiyama, M., Horimoto, N., Ishimaru, T., 2010. Lagrangian observation of phytoplankton dynamics at an artificially enriched subsurface water in Sagami Bay, Japan. J. Oceanogr. 66, 801–813.

Masuda, Y., Yamanaka, Y., Smith, S.L., Hirata, T., Nakano, H., Oka, A., Sumata, H., 2021. Photoacclimation by phytoplankton determines the distribution of global subsurface chlorophyll maxima in the ocean. Commun. Earth Environ. 2, 128.

Mella-Flores, D., Six, C., Ratin, M., Partensky, F., Boutte, C., Le Corguillé, G., Blot, N., Gourvil, P., Kolowrat, C., Garczarek, L., Marie, D., 2012. *Prochlorococcus* and *Synechococcus* have evolved different adaptive mechanisms to cope with light and UV stress. Front. Microbiol. 3.

Moeller, H.V., Laufkötter, C., Sweeney, E.M., Johnson, M.D., 2019. Light-dependent grazing can drive formation and deepening of deep chlorophyll maxima. Nat. Commun. 10, 1978.

Moore, L.R., Goericke, R., Chisholm, S.W., 1995. Comparative physiology of *Synechococcus* and *Prochlorococcus*: influence of light and temperature on growth, pigments, fluorescence and absorptive properties. Mar. Ecol. Prog. Ser. 116, 259–275.

Moore, C.M., Suggett, D.J., Hickman, A.E., Kim, Y.-N., Tweddle, J.F., Sharples, J., Geider, R.J., Holligan, P.M., 2006. Phytoplankton photoacclimation and photoadaptation in response to environmental gradients in a shelf sea. Limnol. Oceanogr. 51, 936–949.

Murty, V.S.N., Gupta, G.V.M., Sarma, V.V., Rao, B.P., Jyothi, D., Shastri, P.N.M., Supraveena, Y., 2000. Effect of vertical stability and circulation on the depth of the chlorophyll maximum in the Bay of Bengal during May–June, 1996. Deep Sea Res. Part I 47, 859–873.

Oxborough, K., 2022. LabSTAF and RunSTAF Handbook 2408-014-HB Issue F. 12.

Oxborough, K., Hanlon, A.R.M., Underwood, G.J.C., Baker, N.R., 2000. In vivo estimation of the photosystem II photochemical efficiency of individual microphytobenthic cells using high-resolution imaging of chlorophyll *a* fluorescence. Limnol. Oceanogr. 45, 1420–1425.

Palmer, M.A., van Dijken, G.L., Greg Mitchell, B., Seegers, B.J., Lowry, K.E., Mills, M.M., Arrigo, K.R., 2013. Light and nutrient control of photosynthesis in natural phytoplankton populations from the Chukchi and Beaufort seas, Arctic Ocean. Limnol. Oceanogr. 58, 2185–2205.

Pérez, V., Fernández, E., Marañón, E., Morán, X.A.G., Zubkov, M.V., 2006. Vertical distribution of phytoplankton biomass, production and growth in the Atlantic subtropical gyres. Deep Sea Res. Part 1 Oceanogr. Res. Pap. 53, 1616–1634.

Platt, T., Gallegos, C.L., 1980. Modelling Primary Production. In: Falkowski, P.G. (Ed.), Primary Productivity in the Sea. Springer, Boston, MA, pp. 339–362.

Prasanth, R., Vijith, V., Vinayachandran, P.N., 2023. Formation, maintenance and diurnal variability of subsurface chlorophyll maximum during the summer monsoon in the southern Bay of Bengal. Prog. Oceanogr. 212, 102974.

Priyadarshi, A., Smith, S.L., Mandal, S., Tanaka, M., Yamazaki, H., 2019. Micro-scale patchiness enhances trophic transfer efficiency and potential plankton biodiversity. Sci. Rep. 9, 17243.

Raateoja, M., Mitchell, B.G., Wang, H., Olivo, E., 2009. Effect of water column light gradient on phytoplankton fluorescence transients. Mar. Ecol. Prog. Ser. 376, 85–101.

Raven, J.A., 1988. The iron and molybdenum use efficiencies of plant-growth with different energy, carbon and nitrogen sources. New Phytol. 109, 279–287.

Ryabov, A.B., Rudolf, L., Blasius, B., 2010. Vertical distribution and composition of phytoplankton under the influence of an upper mixed layer. J. Theor. Biol. 263, 120–133.

Ryan-Keogh, T.J., Thomalla, S.J., Monteiro, P.M.S., Tagliabue, A., 2023. Multidecadal trend of increasing iron stress in Southern Ocean phytoplankton. Science 379, 834–840.
Saijo, Y., Iizuka, S., Asaoka, O., 1969. Chlorophyll maxima in Kuroshio and adjacent area. Mar. Biol. 4, 190–196.
Sathyendranath, S., Platt, T., Stuart, V., Irwin, B.D., Veldhuis, M.J.W., Kraay, G.W., Harrison, W.G., 1996. Some bio-optical characteristics of phytoplankton in the NW Indian Ocean. Mar. Ecol. Prog. Ser. 132, 299–311.
Sato, M., Takeda, S., Furuya, K., 2006. Effects of long-term sample preservation on flow cytometric analysis of natural populations of pico-and nanophytoplankton. J. Oceanogr. 62, 903–908.
Sato, M., Hashihama, F., Kitajima, S., Takeda, S., Furuya, K., 2010. Distribution of nano-sized cyanobacteria in the western and central Pacific Ocean. Aquat. Microb. Ecol. 59, 273–282.
Sato, M., Shiozaki, T., Hashihama, F., Kodama, T., Ogawa, H., Saito, H., Tsuda, A., Takeda, S., Furuya, K., 2022a. Relative depths of the subsurface peaks of phytoplankton abundance conserved over ocean provinces. Limnol. Oceanogr. 67, 2557–2571.
Sato, M., Hirata, K., Shiozaki, T., Takeda, S., 2022b. Effects of iron and light on microbial nitrogen cycles in the primary nitrite maxima of the eastern Indian Ocean. Deep Sea Res. Part I 185, 103808.
Schuback, N., Schallenberg, C., Duckham, C., Maldonado, M.T., Tortell, P.D., 2015. Interacting effects of light and iron availability on the coupling of photosynthetic electron transport and CO_2-assimilation in marine phytoplankton. PLoS One 10, e0133235.
Schuback, N., Oxborough, K., Burkitt-Gray, M., López-García, P., Patey, M.D., Hammermeister, E., Wright, A., Moore, C.M., 2024. Phytoplankton primary productivity: a dual-incubation approach for direct comparison of photosystem II photosynthetic flux (JVPII) and ^{14}C-fixation experiments. Limnol. Oceanogr. Methods 22, 720–737.
Sedwick, P.N., Church, T.M., Bowie, A.R., Marsay, C.M., Ussher, S.J., Achilles, K.M., Lethaby, P.J., Johnson, R.J., Sarin, M.M., McGillicuddy, D.J., 2005. Iron in the Sargasso Sea (Bermuda Atlantic Time-series Study region) during summer: Eolian imprint, spatiotemporal variability, and ecological implications. Global Biogeochem. Cycles 19.
Six, C., Ratin, M., Marie, D., Corre, E., 2021. Marine *Synechococcus* picocyanobacteria: Light utilization across latitudes. Proc. Natl. Acad. Sci. 118, e2111300118.
Suggett, D.J., Moore, C.M., Hickman, A.E., Geider, R.J., 2009. Interpretation of fast repetition rate (FRR) fluorescence: signatures of phytoplankton community structure versus physiological state. Mar. Ecol. Prog. Ser. 376, 1–19.
Sun, P., Sun, K.M., Zhou, Y., Liu, L., Yuan, C., Xu, Z., Li, Y., Zhang, X., Wang, Z., 2024. Changes in size-dependent chlorophyll *a* concentration and group-specific picophytoplankton abundance in short-term nutrient-addition experiments in the Equatorial Eastern Indian Ocean. In: *Frontiers in Marine Science*, p. 11.
Sunda, W.G., Huntsman, S.A., 1997. Interrelated influence of iron, light and cell size on marine phytoplankton growth. Nature 390, 389–392.
Suzuki, K., Liu, H.B., Saino, T., Obata, H., Takano, M., Okamura, K., Sohrin, Y., Fujishima, Y., 2002. East-west gradients in the photosynthetic potential of phytoplankton and iron concentration in the subarctic Pacific Ocean during early summer. Limnol. Oceanogr. 47, 1581–1594.
Thi Dieu Vu, H., Sohrin, Y., 2013. Diverse stoichiometry of dissolved trace metals in the Indian Ocean. Sci. Rep. 3.
Tripathy, S.C., Pavithran, S., Sabu, P., Pillai, H.U.K., Dessai, D.R.G., Anilkumar, N., 2015. Deep chlorophyll maximum and primary productivity in Indian Ocean sector of the Southern Ocean: Case study in the Subtropical and Polar Front during austral summer 2011. Deep Sea Res. Part II 118, 240–249.
Twining, B.S., Rauschenberg, S., Baer, S.E., Lomas, M.W., Martiny, A.C., Antipova, O., 2019. A nutrient limitation mosaic in the eastern tropical Indian Ocean. Deep-Sea Res. Part II: Topical Stud. Oceanography 166, 125–140.
Vaillancourt, R.D., Marra, J., Seki, M.P., Parsons, M.L., Bidigare, R.R., 2003. Impact of a cyclonic eddy on phytoplankton community structure and photosynthetic competency in the subtropical North Pacific Ocean. Deep Sea Res. Part I 50, 829–847.
van den Engh, G.J., Doggett, J.K., Thompson, A.W., Doblin, M.A., Gimpel, C.N.G., Karl, D.M., 2017. Dynamics of *Prochlorococcus* and *Synechococcus* at Station ALOHA revealed through flow cytometry and high-resolution vertical sampling. Front. Mar. Sci. 4.
Varela, R.A., Cruzado, A., Tintore, J., Garcia Ladona, E., 1992. Modelling the deep-chlorophyll maximum: a coupled physical- biological approach. J. Mar. Res. 50, 441–463.
Vaulot, D., Courties, C., Partensky, F., 1989. A simple method to preserve oceanic phytoplankton for flow cytometric analyses. Cytometry 10, 629–635.
Wang, F., Guo, S., Liang, J., Sun, X., 2024. In situ phytoplankton photosynthetic characteristics and their controlling factors in the eastern Indian Ocean. Mar. Pollut. Bull. 198.
Wei, Y., Zhao, X., Sun, J., Liu, H., 2019. Fast repetition rate fluorometry (FRRF) derived phytoplankton primary productivity in the Bay of Bengal. Front. Microbiol. 10.
Weston, K., Fernand, L., Mills, D.K., Delahunty, R., Brown, J., 2005. Primary production in the deep chlorophyll maximum of the central North Sea. J. Plankton Res. 27, 909–922.
Xie, Y., Laws, E.A., Yang, L., Huang, B., 2018. Diel patterns of variable fluorescence and carbon fixation of picocyanobacteria *Prochlorococcus*-dominated phytoplankton in the South China Sea basin. Front. Microbiol. 9.
Yoshikawa, T., Furuya, K., 2008. Phytoplankton photosynthetic parameters and primary production in Japan Sea and the East China Sea: toward improving primary production models. Cont. Shelf Res. 28, 962–976.
Yuan, C., Xu, Z., Zhang, X., Wei, Q., Wang, H., Wang, Z., 2019. Photosynthetic physiologies of phytoplankton in the eastern equatorial Indian Ocean during the spring inter-monsoon. Acta Oceanol. Sin. 38, 83–91.
Yuan, C., Zhang, X., Wang, Z., Li, Y., Xu, Z., Wei, Q., Liu, L., 2021. Latitudinal distribution of the picoplankton community in the eastern equatorial Indian Ocean during the boreal fall intermonsoon period. Deep-Sea Res. Part I: Oceanographic Res. Papers, 168.
Zampollo, A., Cornulier, T., O'Hara Murray, R., Tweddle, J.F., Dunning, J., Scott, B.E., 2023. The bottom mixed layer depth as an indicator of subsurface chlorophyll *a* distribution. Biogeosciences 20, 3593–3611.
Zhu, Y., Ishizaka, J., Tripathy, S.C., Wang, S., Sukigara, C., Goes, J., Matsuno, T., Suggett, D.J., 2017. Relationship between light, community composition and the electron requirement for carbon fixation in natural phytoplankton. Mar. Ecol. Prog. Ser. 580, 83–100.
Zinser, E.R., Lindell, D., Johnson, Z.I., Futschik, M.E., Steglich, C., Coleman, M.L., Wright, M.A., Rector, T., Steen, R., McNulty, N., Thompson, L.R., Chisholm, S.W., 2009. Choreography of the transcriptome, photophysiology, and cell cycle of a minimal photoautotroph, *Prochlorococcus*. PLoS One 4, 18.